HBx-K130M/V131I promotes liver cancer in transgenic mice via AKT/FOXO1 signaling pathway and arachidonic acid metabolism

Amy P Chiu,

State Key Laboratory of Chinese Medicine and Molecular Pharmacology (Incubation), Shenzhen 518057, China; Department of Applied Biology and Chemical Technology, The Hong Kong Polytechnic University, Hong Kong, China

Barbara R Tschida,

Masonic Cancer Center, Department of Pediatrics, Center for Genome Engineering, University of Minnesota, Minneapolis, MN 55455, United States

Tung-Ting Sham,

State Key Laboratory of Chinese Medicine and Molecular Pharmacology (Incubation), Shenzhen 518057, China; Department of Applied Biology and Chemical Technology, The Hong Kong Polytechnic University, Hong Kong, China

Lilian H Lo,

State Key Laboratory of Chinese Medicine and Molecular Pharmacology (Incubation), Shenzhen 518057, China; Department of Applied Biology and Chemical Technology, The Hong Kong Polytechnic University, Hong Kong, China

Branden S Moriarity,

Masonic Cancer Center, Department of Pediatrics, Center for Genome Engineering, University of Minnesota, Minneapolis, MN 55455, United States

Xiao-Xiao Li,

State Key Laboratory of Chinese Medicine and Molecular Pharmacology (Incubation), Shenzhen 518057, China; Department of Applied Biology and Chemical Technology, The Hong Kong Polytechnic University, Hong Kong, China

Regina C Lo,

Department of Pathology, The University of Hong Kong, Hong Kong, China

David E Hinton,

Nicholas School of the Environment, Duke University, United States

Dewi K Rowlands,

Laboratory Animal Services Centre, The Chinese University of Hong Kong, Sha Tin, New Territories, Hong Kong, China

Chi-On Chan,
State Key Laboratory of Chinese Medicine and Molecular Pharmacology (Incubation), Shenzhen 518057, China; Department of Applied Biology and Chemical Technology, The Hong Kong Polytechnic University, Hong Kong, China

Daniel Kam-wah Mok,
State Key Laboratory of Chinese Medicine and Molecular Pharmacology (Incubation), Shenzhen 518057, China; Department of Applied Biology and Chemical Technology, The Hong Kong Polytechnic University, Hong Kong, China

David A Largaespada,
Masonic Cancer Center, Department of Pediatrics, Center for Genome Engineering, University of Minnesota, Minneapolis, MN 55455, United States

Nadia Warner, and
Victorian Infectious Diseases Reference Laboratory, The Peter Doherty Institute for Infection and Immunity, Victoria, Australia

Vincent W Keng
State Key Laboratory of Chinese Medicine and Molecular Pharmacology (Incubation), Shenzhen 518057, China; Department of Applied Biology and Chemical Technology, The Hong Kong Polytechnic University, Hong Kong, China

Abstract

Chronic hepatitis B viral (HBV) infection remains a high underlying cause for hepatocellular carcinoma (HCC) worldwide, while the genetic mechanisms behind this remain unclear. This study elucidated the mechanisms contributing to tumor development induced by the HBV X (HBx) gene of predominantly Asian genotype B HBV and its common HBx variants. To compare the potential tumorigenic effects of K130M/V131I (Mut) and wild-type (WT) HBx on HCC, the *Sleeping Beauty* (*SB*) transposon system was used to deliver HBx Mut and WT into the livers of *fumarylacetoacetate hydrolase* (*Fah*)-deficient mice and in the context of *transformation related protein 53* (*Trp53*) deficiency.

From our results, HBx Mut had a stronger tumorigenic effect than its WT variant. Also, inflammation, necrosis and fibrosis were evident in HBx experimental animals. Reduction of forkhead box O1 (FOXO1) with increased phosphorylation of upstream serine/threonine kinase (AKT) was detected under HBx Mut over-expression. Thus, it is proposed that HBx Mut enhances disease progression by reducing FOXO1 via phosphorylation of AKT. At the metabolomic level, HBx altered the expression of genes that participated in arachidonic acid (AA) metabolism, as a result of inflammation via accumulation of pro-inflammatory factors such as prostaglandins and leukotriene in liver. Taken together, the increased rate of HCC observed in chronic hepatitis B patients with K130M/V131I mutated X protein, may be due to changes in AA metabolism and AKT/FOXO1 signaling.

Keywords

HBV-related HCC; Genetic mechanisms; Cancer metabolism; *Sleeping Beauty* Transposon system; Signaling pathways

Introduction

Liver cancer is the fourth most common cause of cancer related death worldwide, accounting for about 700,000 deaths annually. The major type of primary liver cancer is HCC, which accounts for 85 to 90% of total liver cancer cases (1–3). Chronic HBV infection has been shown to have a strong relationship with liver cirrhosis and HCC (4). HBV infection accounts for more than 50% of all HCC cases globally (5). HBV infection is an endemic disease, in which the prevalence of chronic HBV infection diverges widely in different parts of the world. About 50% of all new liver cancer cases diagnosed were from mainland China (1–3,6,7). HBV is categorized into 10 genotypes (A to J) and various sub-genotypes according to its geographic distributions (3). HBV Genotypes B and C are widely distributed in East and Southeast Asia (3) and are predominantly found in the Han population in mainland China (8).

HBx is encoded by the X open reading frame of HBV. It plays a crucial role in hepatocarcinogenesis, functioning as a transcriptional activator that interacts with nuclear transcription factors and modulates cytoplasmic signalling pathways, such as the RAS/RAF/MAP and WNT/CTNNB1 signalling pathways (9,10). HBx can also promote replication of HBV and regulate biological processes, such as host gene transcription, cell cycle progression, apoptosis, and oxidative stress (3,11,12). HBx has also been reported to induce inflammation, angiogenesis, immune responses and multi-drug resistance, accelerating HCC progression (10,13,14).

Mutations in the HBV genome are very common in chronically infected HBV patients and can be biomarkers for HCC development (15). Several HBx gene mutation hotspots, including A12T, V44I, A66T, H86Y, E109D, and K130M/V131I can be found in HBV carriers. The dual amino acid changes at K130M/V131I, which overlaps both the HBx gene and basal core promoter (BCP), have been consistently shown to have the highest potential to promote HCC progression (10,16–18). HBV patients with chronic hepatitis, fulminant hepatitis or HCC are often detected with mutations at K130M/V131I sites and diagnosed as HBeAg negative (18–20). A recent meta-analysis of 54 studies examining the association between these mutations and HCC showed that X_K130M/V131I are detected in 66.5% of HCC cases, compared to 39.8% of non-HCC cases (21). These X protein changes are encoded by nucleotide changes in the BCP region A1762T/G1764A (BCP_A1762T/G1764A), and have been shown to be associated with decreased PreC/C RNA synthesis and decreased expression of HBeAg (20). However, the effect of the encoded protein changes on the tumorigenic potential of HBx is not well understood. Although several studies have reported the involvement of HBx in HCC development, the differential tumorigenicity of HBx mutations and the genetic mechanism(s) by which HBx induces and/or contributes to

HCC development remains uncertain, and most studies have been performed using transformed liver cell lines such as Huh7.

The *fumarylacetoacetate hydrolase* (*Fah*)-deficient/ *Sleeping Beauty* transposase *11* knock-in (*Fah*/SB11) transgenic mouse model has been established and used to test the oncogenic role of candidate liver cancer genes (9,22–26). This mouse model allows for selective repopulation of hepatocytes with the expression of delivered transgenes. This *Fah*-deficient mouse model has a defect in hydrolysing acetoacetate and fumarate in the tyrosine catabolic pathway. Therefore, it must be treated with nitisinone (NTBC) in the drinking water to prevent tyrosinemia (27). Co-delivery of oncogenes and *Fah* cDNA in a transposon vector and removal of NTBC after gene delivery, the constitutively expressed *SB* transposases recognize and integrate the transposon into the mouse genome in a cut-and paste manner (23). Eventually, *Fah*-deficient hepatocytes will die, while hepatocytes with stable integration and expression of delivered transgenes can survive and repopulate the liver (9,23–25).

The aim of the study reported herein was to discover the impact of K130M/V131I mutant and wild-type variants of HBx-B on HCC progression and explore the genetic mechanism(s) involved with liver tumorigenesis using the *Fah*/SB11 transgenic mouse model.

Methods

Generation of Fah-deficient/Rosa26-SB11 transposase transgenic mice

All animal work was conducted under approved animal welfare protocols of The Chinese University of Hong Kong and The Hong Kong Polytechnic University, Hong Kong, SAR. *Fah*-deficient mice were bred with *Rosa26*-SB$^{Tg/Tg}$ to obtain experimental animals that were deficient for *Fah* and transgenic for *SB* transposase (*Fah*/SB11). All *Fah*-deficient mice were maintained on 6 μg/mL 2-(2-nitro-4-trifluoromethylbenzoyl)-1,3-cyclohexanedione (NTBC, Swedish Orphan International AB, Stockholm, Sweden) in the drinking water until hydrodynamically injected with transposon vector containing the *Fah* cDNA (27). The genotypes of *Fah*/SB11 transgenic mice were confirmed by PCR genotyping using primers specific for *Fah* alleles and *Rosa26*-SB11 as previously described (9).

Plasmid construction

The PCR products of K130M/V131I mutant and wild-type variants of HBx (GOIs) were provided by Dr Nadia Warner. These GOIs were introduced into the Gateway entry clone pENTR 11 Dual Selection Vector (Life Technologies) to produce pENTR-GOI. The GOI in the entry clone was introduced into the destination vector (pT2/GD-DEST-EGFP for *in vivo* experiments or pPB/SB-DEST-EGFP for *in-vitro* experiments) by LR clonase reaction using Gateway LR clonase II Enzyme mix (Life Technologies) to give the pT2/GD-GOI-EGFP or pPB/SB-GOI-EGFP (Supplementary Fig. S1). A short hairpin RNA directed against the *Trp53* gene was also incorporated into a transposon vector (*shp53*) for stable integration into the mouse hepatocyte genome (9,24,25,28) (Supplementary Fig. S1A). All vectors used for hydrodynamic tail vein injections were prepared using EndoFree Plasmid Maxi Kit (Qiagen).

Hydrodynamic tail vein injection

Twenty micrograms of pT2/GD-HBx-B_Mut-EGFP or pT2/GD-HBx-B_WT-EGFP was co-injected with *shp53*-containing plasmid into 45-day old *Fah*/SB11 mice hydrodynamically. After injection, NTBC water was replaced with normal drinking water. The *Fah* cDNA in the expression vectors was co-expressed and allowed for selective repopulation of hepatocytes with stable transposon vector integration. These mice were allowed to age and sacrificed at around 150–200 days post-hydrodynamic injection (PHI) (Supplementary Fig. S1B). Historical controls for pT2/GD-Empty-EGFP with pT2/shp53 were used in this study.

Liver tumor analyses

The whole liver was removed from the euthanized animal, weighed, rinsed, and placed in cold phosphate buffered saline (PBS). The number of liver tumor nodules on rostral and caudal surfaces of all liver lobes were counted and carefully removed using fine forceps and placed in fresh cold PBS. These isolated tumor nodules were then cut into sections for DNA, RNA and protein extraction using a sterile razor blade. Histology sections were taken for larger tumor nodules. Tissue samples for RNA extraction were kept in 200 μL of RNA*later* Stabilization Solution (Life Technologies) and stored at −80°C. DNA extraction was done as described in the PCR genotyping section. RNA was extracted using Trizol reagent (Life Technologies) following the protocol provided by the manufacturer. Protein was extracted using Qproteome Mammalian Protein Prep Kit (Qiagen) following the protocol provided by the manufacturer.

Histological analyses

Formalin-fixed paraffin-embedded liver tissues were processed, sectioned at 5 microns using a standard microtome (Leica), mounted and heat-fixed onto glass slides at 55°C overnight using standard protocols. These tissue slides were then used for hematoxylin and eosin (H&E) staining following standard protocols, and immunohistochemical (IHC) staining as previously described (9). Dilution of primary antibodies used was as follow: pAKT (Ser473) (Cell Signaling Technology (CST)) was diluted in ratio of 1:250, beta-catenin (D10A8) XP (CST) was diluted in ratio of 1:500, Ki67 (Abcam) was diluted in ratio of 1:200, FAH (Abcam) was diluted in ratio of 1:250, p53 (DO-1) (Santa Cruz Biotechnology) was diluted in ratio of 1:100). Board-certified pathologists performed the histopathological analyses.

Semi-quantitative reverse-transcription polymerase chain reaction (RT-PCR)

RNA from liver tissues was extracted using Trizol reagent (Life Technologies) following the protocol provided by the manufacturer. The first strand cDNA was synthesized from 250 ng mRNA using the SuperScript First-Strand Synthesis System for RT-PCR (Life Technologies). Reactions with (RT+) and without (RT-) the reverse transcriptase were performed for all samples. This cDNA was used as template for subsequent PCR with various primer pairs (Supplementary Materials and Methods). PCR conditions were similar to PCR genotyping with reduced cycles to avoid amplicon saturation. Semi-quantitative analyses of unsaturated amplicons were measured using ImageJ software. Intensity of bands was calculated as an arbitrary value relative to *actin, beta* (*Actb*) expression level.

Quantitative RT-PCR

Quantitative RT-PCR (qPCR) was performed to determine the expression level of common downstream genes involved with cancer signaling pathways. The mRNA was extracted as mentioned previously using 1 μg of mRNA as cDNA synthesis template and qPCR was performed using the QuantStudio 7 Flex Real-Time PCR System (University Research Facility in Life Sciences of The Hong Kong Polytechnic University, Hong Kong). PCR reaction mixture consisted of a 1:10 dilution of cDNA in the SYBR Green I containing qPCR master mix (GoTaq qPCR Master Mix, Promega) with specific primers (0.2 μM final concentration of each primer). Primer sequences listed in Supplementary Materials and Methods.

Western blot analyses

Protein was extracted from liver sections of injected mice using Qproteome Mammalian Protein Prep Kit (Qiagen) following the protocol provided by the manufacturer. Protein concentration was detected using standard protein assay (Bio-Rad) and 30 μg of protein was loaded into the SDS-PAGE and transferred onto PVDF membrane. Primary antibodies phospho-AKT, total AKT, non-phospho. (active) CTNNB1, total CTNNB1, FOXO1 and ACTB (CST) were diluted in 5% BSA at 1:1000 concentration. Secondary antibodies (anti-mouse or anti-rabbit) were diluted in 5% BSA at 1:2000 concentration. Membrane was blocked with 5% BSA, then incubated with primary antibody at 4°C overnight followed by secondary antibody incubation at room temperature for an hour. The membrane was then washed with 1× TBST for 3 times in 10 minutes' interval. Afterwards, membrane was visualized using Immobilon Western Chemiluminescent HRP Substrate (Millipore).

Cell culture and AKT inhibitor treatment assay

SNU-449 were cultured with RPMI medium (Gibco, Thermo Fisher) supplemented with 10% heat-inactivated fetal bovine serum (FBS) (Gibco, Thermo Fisher) and 1% Antibiotic-Antimycotic (Anti-Anti) (Gibco, Thermo Fisher). Immortalized human hepatic cell line, HHL7, were cultured with MEM medium supplemented with 10% FBS and 1% Anti-Anti. HHL7 cells (5×10^4 cells) were transfected with 1 μg of pPB/SB-GOI-EGFP and 0.5 μg of transposase vector using ViaFect transfection reagents (Promega) with a plasmid to reagent ratio of 1:3 in 6-well plate (Supplementary Fig. S1C). Puromycin was used for the selection of positively transfected cells. SNU-449 and positively transfected HHL7 cells (4000 cells) were treated with various concentrations (3.125, 6.25, 12.5, 25, 50, 100 and 200 μM) of AKT protein kinase inhibitor (AZD5363, MedChem Express) for 4-days in a 96-well plate. MTS assays were performed using the CellTiter 96 Aqueous One Solution Reagent (Promega) according to the manufacturer's protocol (Supplementary Fig. S1C). Absorbance of each well were measured at 492 nm. Percentage of cell survival were calculated by dividing the absorbance of treated cohorts to the untreated control.

Serum metabolomic analyses

Blood from HBx-B Mut/*shp53*, WT/*shp53* and Empty/*shp53* injected mice was extracted during necropsy, kept at 4°C overnight and serum isolated. The procedure to prepare serum for Ultra Performance Liquid Chromatography-Orbitrap-Mass spectroscopy (UPLC-

Orbitrap-MS), the UPLC separation method and mass spectrometer parameters can be found in supplementary materials (Supplementary Materials and Methods). An equal volume of each serum sample was pooled, vortexed and aliquoted to provide pooled quality control (QC) samples and went through the same extraction protocols of LC-MS as described. They were injected to UPLC-Orbitrap-MS intermittently between samples for stability check of the instruments throughout the runs.

The prepared serum samples were injected into a Waters ACQUITY UPLC system (Waters, Milford, MA, USA). Mass spectrometry analysis was achieved by Thermo Scientific Orbitrap Fusion Lumos Tribrid mass spectrometer equipped with a heated electrospray ionization (H-ESI) interface (Thermo Fisher, Waltham, MA, USA). Data processing was analyzed by Progenesis QI software 2.0 (Nonlinear Dynamics, Newcastle upon Tyne, United Kingdom) and peak area was normalized by all compound with reference of quality control. Quality screening was done by filtering out those unstable metabolites (coefficient of variation > 30% in all pooled quality control samples). The remaining normalized data matrix was exported to the Extended Statistical tool (EZinfo v2.0 software, Umetrics AB) for partial least squares-discriminant analysis (PLS-DA) so as to evaluate their classification performance. The parameter Q^2 is used to assess the goodness of prediction for performance of PLS-DA in a general acceptable threshold value of 0.5. The metabolites that had significant difference between HBx-B Mut/*shp53* and WT/*shp53* experimental samples were identified by comparing their *m/z*, mass fragmentation patterns and chromatographic retention times with commercially available reference standards and/or online metabolite databases such as Human Metabolome Database (http://metlin.scripps.edu), Metlin (http://metlin.scripps.edu) and literatures.

Statistical analyses

Values are given as mean ± standard deviation (SD). Statistical significance was assessed by two-tailed, unpaired Student's *t*-test with *p*-values (Prism Software). *P* values > 0.05 were considered statistically significant.

Results

Divergent effect on tumor burden by mutant and wild-type variants of HBx-B

Expression vectors for pT2/GD-HBx-B_Mut-GFP and pT2/GD-HBx-B_WT-GFP were co-injected with a short hairpin RNA that targeted *Trp53* (*shp53*) into the tail vein of *Fah*/SB11 mice hydrodynamically and the number of GFP-positive tumors counted at around 160-days post hydrodynamic injection (PHI). HBx-B WT/*shp53* and HBx-B Mut/*shp53* variants induced an average tumor burden of 0.14 per mouse and 1.25 per mouse, respectively. HBx-B Mut/*shp53* injected mice ($n = 10$) ($p = 0.1272$) displayed a trend toward higher tumor burden than HBx-B WT/*shp53* counterpart ($n = 10$) (Fig. 1A and 1B). There was a significant difference in liver to whole body weight ratio between HBx-B Mut/*shp53* and HBx-B WT/*shp53* groups ($p = 0.0473$) and both groups had significantly enlarged livers relative to whole body weight ratio of Empty/*shp53* control group ($p < 0.0001$) (Fig. 1C).

Inflammation, proliferation, hepatocytomegaly and necrosis phenotype in HBx injected animals

IHC and H&E stained liver sections displayed hepatic morphological phenotypic changes as a result of HBx over-expression. As expected, normal non-proliferating livers were negative for the cell proliferation marker Ki67 by IHC, while liver tumor nodules isolated from experimental animals injected with HBx-B gene were strongly Ki67-positive (Fig. 1D). Hepatocyte nuclei were enlarged with apparent pyknotic changes, indicating the development of hepatocellular necrosis (Fig. 1E (iii)). Additionally, multi-nuclei and mitotic figures were found in these sections (Fig. 1E (iii) and 1E (iv)). Furthermore, different degrees of inflammation were observed based on the amount of lymphocyte aggregation in the injected liver sections (Fig. 1E (vii)). Histopathological analyses revealed higher inflammation events in livers injected with HBx-B Mut/*shp53* than its corresponding HBx-B WT/*shp53* counterpart (Fig. 2A (i)). A sign of necrosis and degenerative changes were also observed in liver sections of the injected animals (Fig. 2A (ii)). Moreover, mild fibrosis was observed in mice injected with either wild-type or mutant HBx-B gene (Fig. 1E (viii) and Fig. 2A (iii)).

Transcriptional analyses of HBx-B injected liver

To confirm that inflammation and tumor induction were driven by the expression of HBx genes, semi-quantitative RT-PCR was performed to examine the expression of *green fluorescent protein* (*Gfp*), *HBx* and *Fah* transgenes flanked delivered by the transposon vectors. Both normal tissues and tumors isolated from HBx-B Mut/*shp53* and HBx-B WT/ *shp53* mouse liver expressed the *Gfp*, *HBx* and *Fah* transgenes (Fig. 2B), indicating the successful integration and expression of transgenes into the hepatocytes of injected experimental animals. *Alpha-fetoprotein* (*Afp*), a marker for HCC diagnosis, was detected in both HBx-B Mut/*shp53* and HBx-WT/*shp53* groups by semi-quantitative RT-PCR. *Afp* expression level in tumor was higher than that of its corresponding adjacent microscopically normal liver samples ($p = 0.0599$). The mRNA expression levels of *myelocytomatosis oncogene* (*Myc*) and *cyclin D1* (*Ccnd1*), were analyzed in HBx-B/*shp53* injected animals by qPCR. HBx-B WT/*shp53* induced significantly higher expression of *Ccnd1* than Empty/ *shp53*, while there were no significant differences amongst all groups for *Myc* mRNA expression (Fig. 2C). The rescued activity of *Fah* in injected mice was also confirmed by IHC, indicating the successful integration, transcription and translation of genes delivered by the transposon vector (Supplementary Fig. S2A). As expected control wild-type mouse livers were strongly FAH-positive, while non-injected *Fah*/SB11 control animals (under NTBC treatment) were FAH-negative by IHC staining (Supplementary Fig. S2A). There were no detectable TRP53 in either HBx or Empty/*shp53* control cohorts that were co-injected with *shp53* by IHC staining (Supplementary Fig. S2B).

Increased AKT and CTNNB1 protein levels in HBx injected mice

Both *PI3K/AKT* and *WNT/CTNNB1* signaling pathways play vital roles in regulating cellular differentiation, proliferation and survival in HCC. In order to identify underlying mechanisms of HBx-induced HCC, activation of these two pathways were examined. Western blot analyses were performed on protein extracted from experimental cohorts using

non-phospho. (active) CTNNB1 (active CTNNB1), CTNNB1, phopho-AKT (ser473) (pAKT), AKT and FOXO1 primary antibodies (Fig. 2D). The protein levels of total CTNNB1 and total AKT were significantly higher in HBx-B Mut/*shp53* than that of Empty/ *shp53*, while FOXO1 protein level was significantly lower in HBx-B Mut/*shp53* than that of Empty/*shp53*, and there were a trend showing higher protein level of active CTNNB1and phospho-AKT in HBx-B Mut/*shp53* than that of Empty/*shp53* (Fig. 2D, left panel). However, only phospho-AKT protein level was significantly increased in HBx-B WT/*shp53* than that of Empty/*shp53* and there was no significant difference in pAKT, active and total CTNNB1 and FOXO1 levels between HBx-B WT/*shp53* and Empty/*shp53* (Fig. 2D, right panel). Furthermore, IHC of liver tumor nodules isolated from mice injected with HBx-B Mut/*shp53* and HBx-WT/*shp53* groups were strongly positive for nuclear pAKT and membranous active CTNNB1 (Supplementary Fig. S2C and S2D). The effect of suppressing AKT signaling pathway on cell survival was performed on SNU-449, a HBV-positive liver cancer cell line, and immortalized human hepatic cell line HHL7 transfected with HBx genotype B mutant and wild-type genes. Treatment with AKT inhibitor AZD5363 could significantly reduce the survival rate of SNU-449 and HBx transfected HHL7 cell lines compared to non-treated cells (Fig. 2E).

RNA-seq revealed crucial roles of metabolomic reprogramming in HBx-B injected mice

RNA-seq was performed to quantify the RNA expression profile of HBx-B injected animals. RNA from HBx-B Mut/*shp53* tumors ($n = 3$) and normal tissues ($n = 4$), HBx-WT/*shp53* normal tissues ($n = 3$) and Empty/*shp53* normal tissues ($n = 3$) were analyzed by Illumina sequencing and expression level of each gene was calculated by fragments per kilobase of exon per million reads mapped (FPKM). Raw RNA-seq data was uploaded to Sequence Read Archive (SRA) with the accession number PRJNA529044. Based on the gene expression level, differentially expressed genes (DEGs) were identified between groups. Fold-change in gene expression between 2 samples was calculated by log 2 FPKM ratio of 2 samples. Significant gene expression difference was filtered with log 2 ratio greater or equal to 1 (for up-regulation) and smaller or equal to −1 (for down-regulation).

The number of DEGs between the normal tissues of HBx-B Mut/*shp53* against Empty/*shp53* control, HBx-B WT/*shp53* against Empty/*shp53* control and HBx-B Mut/*shp53* against HBx-B WT/*shp53* were low (Supplementary Fig. S3A). Comparing RNA expression profiles of tumors ($n = 3$) and normal ($n = 4$) tissues of HBx-B Mut injected mice, 377 DEGs were totally identified: 235 genes were up-regulated and 142 genes were down-regulated in the tumor compared to its normal tissues (Supplementary Fig. S3A and S3B). *Insulin growth factor 2* (*Igf2*), *Rous sarcoma oncogene* (*Src*), *p21 (RAC1) activated kinase 6* (*Pak6*), as well as well-known oncogenes *Myc* and *matrix metallopeptidases* (*Mmps*) were up-regulated in the tumors from the HBx-B Mut/*shp53* cohort (Fig. 3 and Supplementary Table S1). Transcriptional mRNA expression of targeted genes, such as *insulin growth factor 2* (*Igf2*), *Src*, *Pak6* and *Mmp7* were further confirmed by qPCR in non-sequenced tumor ($n = 5$) and normal ($n = 5$) samples. Significant up-regulation of these targeted genes was detected in HBx-B injected cohorts compared with the Empty/*shp53* control (Fig. 4A). Using KEGG pathway analyses, the DEGs show significant alterations for both canonical signaling and metabolic pathways. Among the canonical signaling pathways, most of the

DEGs were involved in common cancerous signal transduction pathways such as Ras signaling, PI3K-Akt signaling, ECM-receptor interaction, and mitogen activated protein kinase (MAPK) signaling, and Notch signaling (Supplementary Table S2).

Apart from the canonical signaling pathways, a large number of genes were associated with various metabolic pathways (59/519 genes). This suggests that metabolic changes played a significantly important role in promoting tumor progression. Arachidonic acid (AA) metabolism is one of the metabolic pathways with the highest number of DEGs involved (13 DEGs) (Fig. 3 and Supplementary Table S2). DEGs involved in AA metabolism, including *prostaglandin-endoperoxide synthase 2* (*Ptgs2*), *secretory phospholipase A2* (*Pla2g*) and *arachidonate 12-lipoxygenase* (*Alox12*) were up-regulated, while cytochrome p450 monooxygenase, such as *Cyp2* and *Cyp4f*, genes encoding xenobiotic monooxygenase and leukotriene-B4 (LTB_4) 20-monooxygenase were down-regulated (Fig. 3 and Supplementary Table S1). The abundance of metabolites, such as prostaglandin B2, D2 and E2, LTB_4 and 12-hydroxyeicosatetraenoic acid (12-HETE), from AA metabolism were shown to be significantly higher in the HBx genotype B mutant and wild-type experimental cohorts compared with the Empty/*shp53* control (Fig. 4B).

Serum metabolomics analyses using UPLC-Orbitrap-MS

Since the RNA-seq results indicated metabolic disorder was highly associated with tumor development in HBx-B injected mice. Therefore, serum samples from experimental mice were used to perform metabolomics analysis using UPLC-Orbitrap-MS to determine metabolic changes in the context of HBx over-expression. Fold-changes of metabolites were compared between mutant and wild-type cohorts. A significantly higher abundance of xanthine (67.23-fold increase), as well as its downstream metabolites urate (2.15-fold increase) and 5-hydroxyisourate (3.55-fold increase) were detected in mutant cohort compared to its wild-type cohort (Fig. 3 and Supplementary Fig. S4B). These metabolites are produced during the break down of tumor cells (29), providing further evidence of the involvement of HBx-B mutant gene in liver tumorigenesis. Furthermore, metabolites 9,10-dihydroxy-12*Z*-octadecenoic acid (9,10-DiHOME) and 12,13-dihydroxy-9*Z*-octadecenoic acid (12,13-DiHOME) involved in linoleic acid metabolism were significantly reduced ($p < 0.05$) in mutant serum than that in wild-type serum. Both serum metabolites abundance and RNA expression level of *Cyp2C* and *Cyp2e1*, genes encoding enzymes that break down linoleic acid, were down-regulated (Fig. 3 and Supplementary Fig. S4B). Additionally, the ion abundances of metabolites, such as taurocholate (TCA), taurochenodeoxycholate (TCDCA) and taurohyodeoxycholate (THDCA)/tauroursodeoxycholate (TUDCA), in the synthesis of bile acids (BAs) from cholesterol were significantly reduced in the mutant cohort compared to its wild-type cohort. This finding was consistent with the RNA-seq result that the expression level of *Cyp7a1*, which encodes the key enzyme that converts cholesterol to BAs, was significantly down-regulated (Fig. 3 and Supplementary Fig. S4B).

Discussion

Using the *Fah*/SB11 mouse model, K130M/V131I mutant variant of HBx-B induced a higher tumor burden than its wild-type counterpart and significantly increased the liver

weight of the experimental animals. Hepatocytes of HBx-B Mut/*shp53* and WT/*shp53* injected mice were larger than those of Empty/*shp53* control and *Fah*/SB11 non-injected mice, indicating hepatomegaly. In another experimental cohort in which *Fah*/SB11 mice were injected with HBx-B Mut and WT alone, the number of tumors induced were similar to the experimental cohorts that were co-injected with *shp53* (*data not shown*). Based on this evidence, inactivation of *Trp53* did not contribute to tumorigenesis at time of necropsy (between 160 to 200 PHI).

In addition, severe inflammation, mild necrosis and fibrosis were observed in livers injected with HBx-B Mut/*shp53* indicating the development of chronic hepatitis. From the RNA-seq analyses, the AA metabolism pathway associated with pro-inflammatory process was activated. From the metabolite profiles of the experimental cohorts, significantly higher abundance of the pro-inflammatory factors, such as prostaglandin B2, D2, E2, LTB$_4$ and the pro-carcinogenic factor, 12-HETE, from AA metabolism was detected in the HBx mutant and wild-type experimental cohorts compared with the Empty/*shp53* control (Fig. 4B). These results suggest that HBx-B could induce liver inflammation through the activation of the AA metabolism pathway, producing more pro-inflammatory factors and attract the accumulation of leukocytes into the liver tissues.

Both IHC and Western blot analyses confirmed expression of either HBx-B Mut or WT could activate phosphorylation of AKT and overexpress CTNNB1 in our injected mice. Moreover, the protein level of FOXO1 was significantly reduced in HBx-B Mut/*shp53* group. FOXO1 is a transcriptional factor that mediates the expression of downstream target genes involved in cell proliferation, apoptosis, cell cycle arrest and metabolism (30,31). FOXO1 is also a downstream target of AKT, which can be phosphorylated by pAKT and translocated to the cytoplasm, and subsequently degraded via ubiquitination (30). Therefore, we proposed that HBx-B mutant variant increased cell proliferation and promoted cell cycle progression by activating AKT phosphorylation, which in turn, phosphorylated and translocated FOXO1 to cytoplasm for ubiquitination, resulting in reduced FOXO1 abundance in cells. In transcriptional analysis, both HBx-B Mut/*shp53* and WT/*shp53* induced over-expression of *Afp, Myc* and *Ccnd1*.

RNA-seq was performed to quantify the RNA expression profiles between tumor and its peripheral normal tissue of HBx-B Mut injected mice. The sequencing results highlighted the importance of signal transduction pathways, such as PI3K-Akt signaling pathway, and metabolic pathways, including AA metabolism. The mRNA expression levels of *Igf2*, *Src*, *Pak6*, and *Mmps* were significantly increased in tumor of HBx-B Mut/*shp53* injected animals comparing to that of normal tissues. *Igf2* encodes for a mitogenic peptide, namely insulin-like growth factor 2 (IGF2). Other IGF components such as IGF2 mRNA binding protein (IGF2BP) and IGF binding proteins (IGFBPs) are required to initiate the signaling cascade of IGF2 (32). Ingenuity Pathway Analysis upstream regulator analyses showed that expression of *Igf2* is regulated by CTNNB1 and PI3K/AKT (Supplementary Table S3). In addition, *Igfbp1*, which was also up-regulated in tumors of HBx-B Mut/shp53 cohort, is regulated by FOXO1 (Supplementary Table S3). These results are consistent with our translational and transcriptional analyses and further confirmed the activity of AKT/FOXO1 signaling pathway on regulating cell growth, proliferation and survival via IGF2. Up-

regulation of *IGF2* was significantly associated with risk of hepatoblastoma development (32). Based on a previous study on gene expression profiling of HCC patients acquired from various risk factors, *IGF2* was one of the differentially expressed gene found exclusively in HBV-induced HCC cases (33). Activation of AKT and up-regulation of *Src* in the HBx-B Mut cohort triggered downstream-cascaded events resulting in up-regulation and activation of mDia1, which is responsible for actin regulation and associated with cell motility. A recent study had published that high level of Src could promote cell proliferation and invasion (34). Additionally, protein tyrosine kinase 2 (PTK2)/Src complex could also activate MAPK, WNT and PI3K-AKT signaling pathways that are responsible for cell proliferation and cell survival by overexpressing oncogenes such as *Myc* and *Mmps*, which were also up-regulated in our DEGs list. Furthermore, Src is also an up-stream target of PAK, which is encoded by *Pak6* and is an effector of RAC proteins. Activation of Rac cascade triggers actin polymerization and induce membrane protrusion and cell spreading, resulting in mesenchymal cell morphology (35). PAK also possesses oncogenic roles that can regulate cell proliferation, cell survival, adhesion and migration (36).

DEGs involved in AA metabolism were affected significantly, *Ptgs2*, *Pla2g* and *Alox12* were up-regulated, while *Cyp2*, *Cyp4f*, genes encoding xenobiotic monooxygenase and LTB_4 20-monooxygenase were down-regulated. As mentioned previously, AA metabolism is highly associated with inflammation events in liver (37,38). Thus, it is hypothesized that HBx Mut could induce severe inflammation in liver via AA metabolism pathway by up-regulating expression of *Ptgs2*, which encodes for prostaglandin-endoperoxide synthase that converts the unstable product prostaglandin G_2 (PGG_2) to prostaglandin H_2 (PGH_2), that would be further converted to other prostaglandins (PGs), including PGE_2, PGD_2 and PGB_2, resulting in over-production of pro-inflammatory factors. Studies have shown that these PGs can promote tumor growth and are highly abundant in colon, lung, breast and head and neck cancers (39–43). In addition, accumulated PGs could activate RAS/ERK and glycogen synthase kinase 3 beta (GSK3B)/CTNNB1 signaling pathways and hence induce cell proliferation (39). On the other hand, gene encoding LTB_4 20-monooxygenase was down-regulated. LTB_4 20-monooxygenase is an enzyme that converts LTB_4 to 20-OH-LTB_4, the down-regulation of gene encoding LTB_4 20-monooxygenase caused the accumulation of LTB_4 in cells. LTB_4 is also known to be a pro-inflammatory factor that attracts leukocytes to the injured tissue (44). Moreover, LTB_4 could also activate MEK/ERK and PI3K/AKT pathways through the interaction with the G protein-coupled receptors BLT2 in human pancreatic cancer cells (45,46). Furthermore, ALOX12 has been described as a potential pro-carcinogenic enzyme (39). The higher abundance of 12-HETE, product of ALOX12, was detected in HBx-B injected experimental cohorts compared with Empty/*shp53* control, suggesting that HBx gene might also promote tumor progression by up-regulation of *Alox12*.

All results shown here confirm that HBx-B K130M/V131I mutant variant displayed a stronger tumorigenic effect than its wild-type counterpart. The X_K130M/V131I amino acid changes are encoded by nucleotide changes at BCP_A1762T/G1764A, which also result in a decrease in PC/C mRNA and subsequent HBeAg expression. These changes have been strongly associated with the development of HCC in many clinical studies, however whether the increased HCC is associated with the decrease in HBeAg levels, or mutation of the X

protein remains unknown. To our knowledge, this is the first study to show a direct effect of these X mutations on HBx-associated tumorigenesis. We suggest that HBx-B mutant variant promoted tumor progression via phosphorylation of AKT in PI3K/AKT signaling pathway and reduced FOXO1 production, resulting in up-regulation of *Igf2*. Moreover, it significantly altered the metabolism of arachidonic acid, which contributed to inflammation of HBx-B injected animals. HBx Mut induced inflammation via AA metabolism by accumulation of pro-inflammatory factors such as the different types of PGs, LTB_4 and 12-HETE to the infected tissues (Fig. 5) (47). Taken together, these results provide a potential mechanism whereby HBV encoding X_K130M/V131I (BCP_A1762T/G1764A) may contribute to the high rate of HCC observed clinically in patient cohorts containing these mutations.

Supplementary Material

Refer to Web version on PubMed Central for supplementary material.

Financial support statement:

Bibliography

1. Venook AP, Papandreou C, Furuse J, de Guevara LL. The incidence and epidemiology of hepatocellular carcinoma: a global and regional perspective. Oncologist 2010;15 Suppl 4:5–13

2. El-Serag HB. Epidemiology of viral hepatitis and hepatocellular carcinoma. Gastroenterology 2012;142:1264–73e1 [PubMed: 22537432]

3. Zhang Q, Cao G. Genotypes, mutations, and viral load of hepatitis B virus and the risk of hepatocellular carcinoma: HBV properties and hepatocarcinogenesis. Hepat Mon 2011;11:86–91 [PubMed: 22087123]

4. Di Bisceglie AM. Hepatitis B and hepatocellular carcinoma. Hepatology 2009;49:S56–60 [PubMed: 19399807]

5. Lupberger J, Hildt E. Hepatitis B virus-induced oncogenesis. World J Gastroenterol 2007;13:74–81 [PubMed: 17206756]

6. Cao GW. Clinical relevance and public health significance of hepatitis B virus genomic variations. World journal of gastroenterology : WJG 2009;15:5761–9 [PubMed: 19998495]

7. Ferlay J, Soerjomataram I, Dikshit R, Eser S, Mathers C, Rebelo M, et al. Cancer incidence and mortality worldwide: sources, methods and major patterns in GLOBOCAN 2012. Int J Cancer 2015;136:E359–86 [PubMed: 25220842]

8. Zhang Q, Liao Y, Chen J, Cai B, Su Z, Ying B, et al. Epidemiology study of HBV genotypes and antiviral drug resistance in multi-ethnic regions from Western China. Sci Rep 2015;5:17413 [PubMed: 26612031]

9. Keng VW, Tschida BR, Bell JB, Largaespada DA. Modeling hepatitis B virus X-induced hepatocellular carcinoma in mice with the Sleeping Beauty transposon system. Hepatology 2011;53:781–90 [PubMed: 21374658]

10. Ng SA, Lee C. Hepatitis B virus X gene and hepatocarcinogenesis. J Gastroenterol 2011;46:974–90 [PubMed: 21647825]

11. Gong DY, Chen EQ, Huang FJ, Leng XH, Cheng X, Tang H. Role and functional domain of hepatitis B virus X protein in regulating HBV transcription and replication in vitro and in vivo. Viruses 2013;5:1261–71 [PubMed: 23698398]

12. Ghany M, Liang TJ. Drug targets and molecular mechanisms of drug resistance in chronic hepatitis B. Gastroenterology 2007;132:1574–85 [PubMed: 17408658]

13. Liu LP, Liang HF, Chen XP, Zhang WG, Yang SL, Xu T, et al. The role of NF-kappaB in Hepatitis b virus X protein-mediated upregulation of VEGF and MMPs. Cancer Invest 2010;28:443–51 [PubMed: 20073580]

14. Neuveut C, Wei Y, Buendia MA. Mechanisms of HBV-related hepatocarcinogenesis. J Hepatol 2010;52:594–604 [PubMed: 20185200]

15. Caligiuri P, Cerruti R, Icardi G, Bruzzone B. Overview of hepatitis B virus mutations and their implications in the management of infection. World J Gastroenterol 2016;22:145–54 [PubMed: 26755866]

16. Lindh M, Gustavson C, Mardberg K, Norkrans G, Dhillon AP, Horal P. Mutation of nucleotide 1,762 in the core promoter region during hepatitis B e seroconversion and its relation to liver damage in hepatitis B e antigen carriers. J Med Virol 1998;55:185–90 [PubMed: 9624604]

17. Lin X, Xu X, Huang QL, Liu YQ, Zheng DL, Chen WN, et al. Biological impacts of "hot-spot" mutations of hepatitis B virus X proteins are genotype B and C differentiated. World journal of gastroenterology : WJG 2005;11:4703–8 [PubMed: 16094714]

18. Lin CL, Liao LY, Wang CS, Chen PJ, Lai MY, Chen DS, et al. Basal core-promoter mutant of hepatitis B virus and progression of liver disese in hepatitis B e antigen-negative chronic hepatitis B. Liver Int 2005;25:564–70 [PubMed: 15910494]

19. Kuang SY, Jackson PE, Wang JB, Lu PX, Munoz A, Qian GS, et al. Specific mutations of hepatitis B virus in plasma predict liver cancer development. Proc Natl Acad Sci U S A 2004;101:3575–80 [PubMed: 14990795]

20. Datta S, Chatterjee S, Veer V, Chakravarty R. Molecular biology of the hepatitis B virus for clinicians. J Clin Exp Hepatol 2012;2:353–65 [PubMed: 25755457]

21. Yang Z, Zhuang L, Lu Y, Xu Q, Tang B, Chen X. Naturally occurring basal core promoter A1762T/G1764A dual mutations increase the risk of HBV-related hepatocellular carcinoma: a meta-analysis. Oncotarget 2016;7:12525–36 [PubMed: 26848866]

22. Chiu AP, Tschida BR, Lo LH, Moriarity BS, Rowlands DK, Largaespada DA, et al. Transposon mouse models to elucidate the genetic mechanisms of hepatitis B viral induced hepatocellular carcinoma. World J Gastroenterol 2015;21:12157–70 [PubMed: 26576100]

23. Bell JB, Podetz-Pedersen KM, Aronovich EL, Belur LR, McIvor RS, Hackett PB. Preferential delivery of the Sleeping Beauty transposon system to livers of mice by hydrodynamic injection. Nat Protoc 2007;2:3153–65 [PubMed: 18079715]

24. Keng VW, Sia D, Sarver AL, Tschida BR, Fan D, Alsinet C, et al. Sex bias occurrence of hepatocellular carcinoma in Poly7 molecular subclass is associated with EGFR. Hepatology 2013;57:120–30 [PubMed: 22899566]

25. Keng VW, Villanueva A, Chiang DY, Dupuy AJ, Ryan BJ, Matise I, et al. A conditional transposon-based insertional mutagenesis screen for genes associated with mouse hepatocellular carcinoma. Nat Biotechnol 2009;27:264–74 [PubMed: 19234449]

26. Riordan JD, Keng VW, Tschida BR, Scheetz TE, Bell JB, Podetz-Pedersen KM, et al. Identification of rtl1, a retrotransposon-derived imprinted gene, as a novel driver of hepatocarcinogenesis. PLoS Genet 2013;9:e1003441 [PubMed: 23593033]

27. Grompe M, al-Dhalimy M, Finegold M, Ou CN, Burlingame T, Kennaway NG, et al. Loss of fumarylacetoacetate hydrolase is responsible for the neonatal hepatic dysfunction phenotype of lethal albino mice. Genes Dev 1993;7:2298–307 [PubMed: 8253378]

28. Wangensteen KJ, Wilber A, Keng VW, He Z, Matise I, Wangensteen L, et al. A facile method for somatic, lifelong manipulation of multiple genes in the mouse liver. Hepatology 2008;47:1714–24 [PubMed: 18435462]

29. Tiu RV, Mountantonakis SE, Dunbar AJ, Schreiber MJ Jr. Tumor lysis syndrome. Semin Thromb Hemost 2007;33:397–407 [PubMed: 17525897]

30. Xing YQ, Li A, Yang Y, Li XX, Zhang LN, Guo HC. The regulation of FOXO1 and its role in disease progression. Life Sci 2018;193:124–31 [PubMed: 29158051]

31. Wang Y, Zhou YM, Graves DT. FOXO Transcription Factors: Their Clinical Significance and Regulation. Biomed Res Int 2014

32. Brouwer-Visser J, Huang GS. IGF2 signaling and regulation in cancer. Cytokine Growth Factor Rev 2015;26:371–7 [PubMed: 25704323]

33. Marshall A, Lukk M, Kutter C, Davies S, Alexander G, Odom DT. Global gene expression profiling reveals SPINK1 as a potential hepatocellular carcinoma marker. PLoS One 2013;8:e59459 [PubMed: 23527199]

34. Tavares S, Vieira AF, Taubenberger AV, Araujo M, Martins NP, Bras-Pereira C, et al. Actin stress fiber organization promotes cell stiffening and proliferation of pre-invasive breast cancer cells. Nat Commun 2017;8:15237 [PubMed: 28508872]

35. Nakamura F FilGAP and its close relatives: a mediator of Rho-Rac antagonism that regulates cell morphology and migration. Biochem J 2013;453:17–25 [PubMed: 23763313]

36. Radu M, Semenova G, Kosoff R, Chernoff J. PAK signalling during the development and progression of cancer. Nature Reviews Cancer 2014;14:13–25 [PubMed: 24505617]

37. Gai Z, Visentin M, Gui T, Zhao L, Thasler WE, Hausler S, et al. The effects of farnesoid X receptor activation on arachidonic acid metabolism, NF-kB signaling and hepatic inflammation. Mol Pharmacol 2018

38. Ricciotti E, FitzGerald GA. Prostaglandins and Inflammation. Arterioscl Throm Vas 2011;31:986–1000

39. Wang D, Dubois RN. Eicosanoids and cancer. Nat Rev Cancer 2010;10:181–93 [PubMed: 20168319]

40. Hambek M, Baghi M, Wagenblast J, Schmitt J, Baumann H, Knecht R. Inverse correlation between serum PGE2 and T classification in head and neck cancer. Head Neck-J Sci Spec 2007;29:244–8

41. McLemore TL, Hubbard WC, Litterst CL, Liu MC, Miller S, McMahon NA, et al. Profiles of prostaglandin biosynthesis in normal lung and tumor tissue from lung cancer patients. Cancer Res 1988;48:3140–7 [PubMed: 3130187]

42. Rigas B, Goldman IS, Levine L. Altered eicosanoid levels in human colon cancer. J Lab Clin Med 1993;122:518–23 [PubMed: 8228569]

43. Wang D, Dubois RN. Cyclooxygenase-2: a potential target in breast cancer. Semin Oncol 2004;31:64–73

44. Saeki K, Yokomizo T. Identification, signaling, and functions of LTB4 receptors. Semin Immunol 2017;33:30–6 [PubMed: 29042026]

45. Azrad M, Turgeon C, Demark-Wahnefried W. Current evidence linking polyunsaturated Fatty acids with cancer risk and progression. Front Oncol 2013;3:224 [PubMed: 24027672]

46. Tong WG, Ding XZ, Talamonti MS, Bell RH, Adrian TE. LTB4 stimulates growth of human pancreatic cancer cells via MAPK and PI-3 kinase pathways. Biochem Biophys Res Commun 2005;335:949–56 [PubMed: 16105664]

47. Sidiropoulos K, Viteri G, Sevilla C, Jupe S, Webber M, Orlic-Milacic M, et al. Reactome enhanced pathway visualization. Bioinformatics 2017;33:3461–7 [PubMed: 29077811]
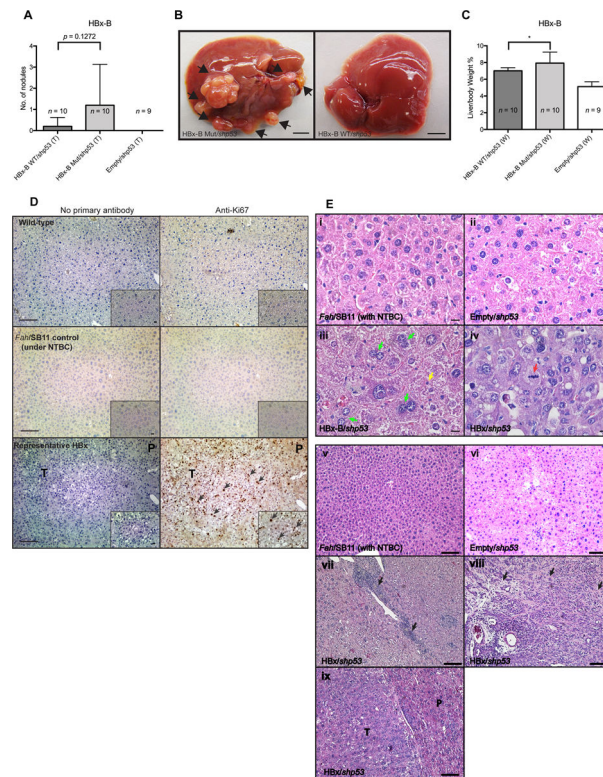
Implications: Our findings suggested that HBx-K130M/V131I mutant variant promoted HCC progression by activating AKT/FOXO1 pathway and inducing stronger inflammation in liver via arachidonic acid metabolism.

Fig. 1. Tumor burdens in *Fah*/SB11 mice injected with wild-type (WT) and mutant (Mut) variants of HBx-B genotypes.

(A) Number of tumors found in experimental animals at about 160-days post-hydrodynamic injection (HBx-B WT/shp53 (T), $n = 10$; HBx-B Mut/shp53 (T), $n = 10$; Empty/shp53 (T), $n = 9$). All mice were co-injected with *shp53*. Mean ± S.D.; *n*, number of animals; *p*, unpaired student *t*-test. **(B)** Liver to whole body weight ratio of experimental animals. Mean ± S.D.; *n*, number of animals; *p*, unpaired student *t*-test. **(C)** Representative image demonstrating diverse tumor burden observed in the HBx-B Mut/shp53 and HBx-B WT/shp53 experimental animals. Arrows indicate tumor nodules; the orientation of the livers were optimized to show the most tumor nodules; scale bars, 0.5 cm. Levels of pathological events were graded from 0 to 3, in which grade 0 was the least severe; while grade 3 was the most severe. **(D)** Representative H&E staining images demonstrating dysplastic hepatocyte morphology of the experimental animals. **(i, v)** Non-injected *Fah*/SB11 liver under continuous treatment of NTBC showing normal hepatocyte morphology. **(ii, vi)** *Fah*/SB11 liver injected with empty vector control in the context of *shp53*. **(iii)** Multinucleated cells (indicated with green arrow) and pyknotic nuclei (indicated with yellow arrow) of hepatocytes were found in HBx/*shp53* injected liver. **(iv)** More mitotic figures (indicated with red arrow) were noted in liver sections injected with HBx/*shp53*. Scale bars, 11 µm. **(vii)** Fibrosis observed in *Fah*/SBll animals with HBx-B genotype co-injected with *shp53*. **(viii)** Areas of lymophocytic inflammation (arrows) seen in *Fah*/SBll mice with HBx gene with co-injection of *shp53*. **(ix)** Tumor nodule (T) observed in *Fah*/SBll animals HBx gene co-injected with *shp53* with dysplastic hepatic morphology seen in peripheral hepatocytes (P). Scale bars, 100 µm. **(E)** Representative IHC images for anti-Ki67 staining in controls and liver tumors of *Fah*/SB11 animal injected with various HBx and *shp53* transgenes. Left

column, no primary antibody was used. Right column, anti-Ki67 primary antibody used. Top and Middle panels, wild-type mouse liver and non-injected *Fah*/SB11 liver from animal under the treatment of NTBC water showing no detectable Ki67 activity, respectively. Bottom panels, *Fah*/SB11 animal injected with HBx-B Mut/*shp53* shown strong nuclear staining of Ki67 in both tumor (T) and peripheral tissue (P) area. Scale bars, 100 μm. Magnified image was shown in right corner (solid-lined box) of each slide. Scale bars, 11 μm.
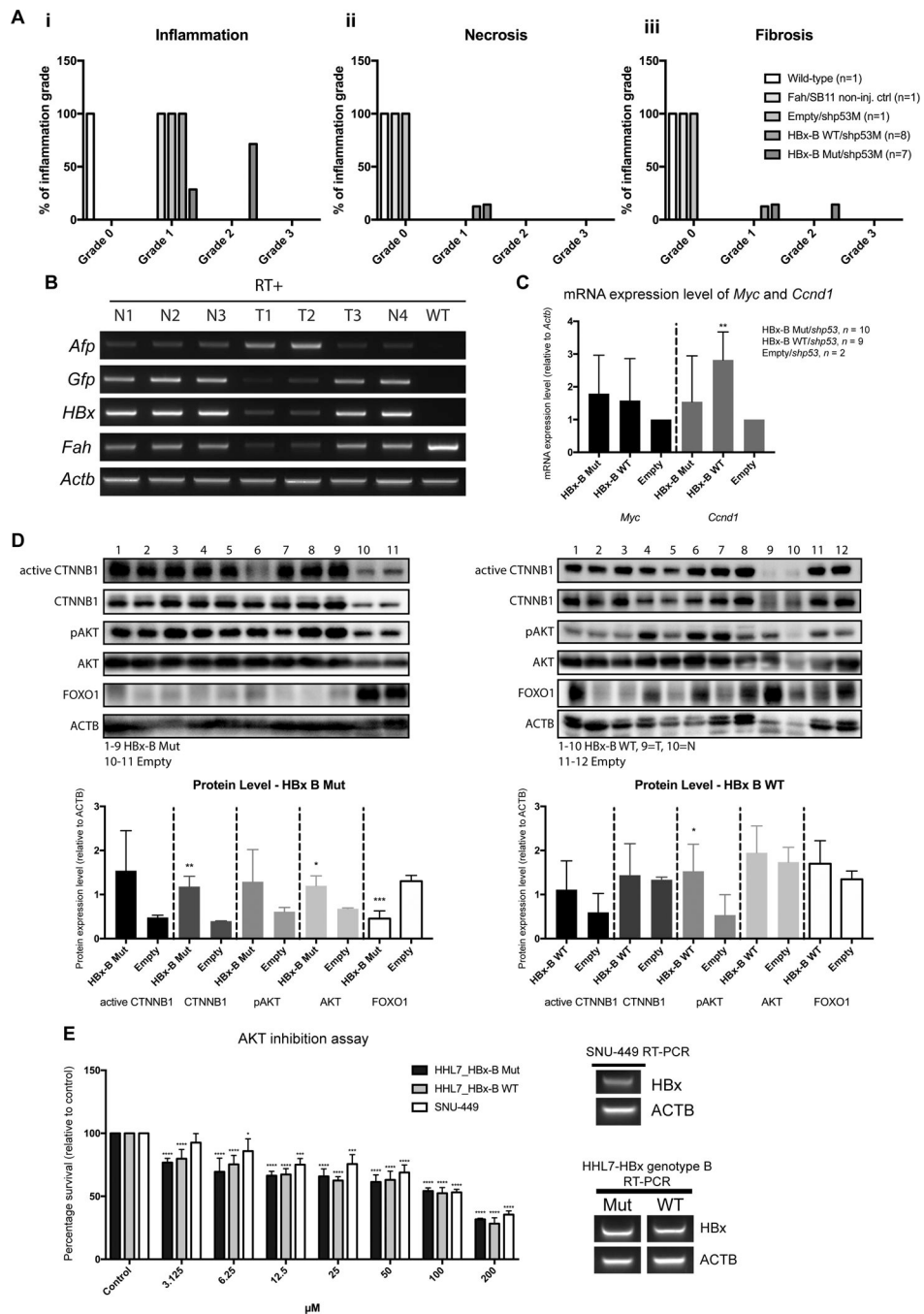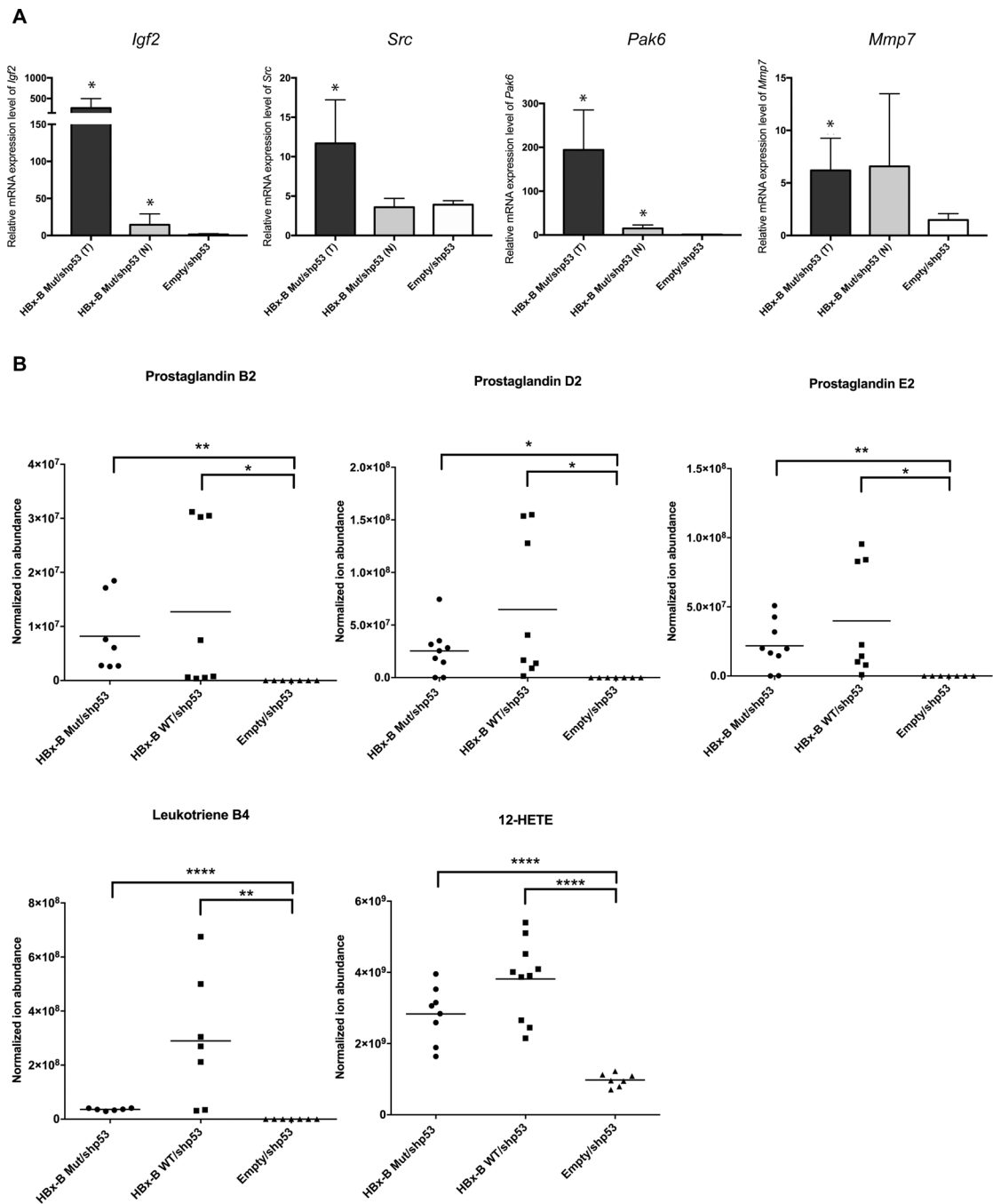
Fig. 2. Histopathological changes and evidence of AKT signaling involvement in hepatocytes of HBx injected animals.

(**A**) Histopathology of livers injected with HBx-B Mut/*shp53* and HBx-B WT/*shp53*. **(i)** Occurrence of inflammation, **(ii)** necrosis, and **(iii)** fibrosis. (**B**) RT-PCR of liver and tumor samples from representative experimental animals. RT-negative controls gave no detectable bands at similar PCR cycle numbers for each gene tested (*data not shown*). N, peripheral normal tissue; T, tumor tissue; WT, normal wild-type adult liver. **(C)** qPCR on mRNA expression level of *Myc* and *Ccnd1* in HBx-B Mut/*shp53* and HBx-B WT/*shp53*

experimental animals. **(D)** Representative Western blot analyses of proteins extracted from liver of *Fah*/SB11 mice injected with HBx-B Mut/*shp53* (**left panel**) and HBx-B WT/*shp53* (**Right panel**) using Non-phospho (active) CTNNB1, CTNNB1, pAKT, AKT, FOXO1 and ACTB antibodies **(Top panels)** and its semi-quantitatve protein level with respect to its corresponding ACTB level **(Bottom panels)**. Mean ± S.D.; *p*, unpaired student *t*-test, *, *p* 0.05, **, *p* 0.01, ***, *p* 0.001. **(E)** Survival rate of HBx expressing cell lines under different concentrations of AKT protein kinase inhibitor (AZD5363). Mean ± S.D.; *p*, ordinary one-way ANOVA, *, *p* 0.05, ***, *p* 0.001, ****, *p* 0.0001. Representative RT-PCR analyses for the HBx genes in SNU-449 and transfected HHL7 cells.

Fig. 3. The schematic summary of molecular pathways induced by HBx-B genes.
Asterisk (*) represent metabolites changes detected by UPLC-MS in serum of HBx-B
experimental animals. Up arrows represent up-regulated DEGs, and down arrows represent
down-regulated DEGs.

A

B

Fig. 4. Expression level validation of targeted DEGs and metabolite profiles of AA metabolism pathway.

(**A**) Relative mRNA expression level of *Igf2, Src, Pak6* and *Mmp7* were shown to be significantly up-regulated in tumors of HBx-B Mut/shp53 injected cohort compared with empty control. Mean ± S.D.; *p*, unpaired student *t*-test, *, *p* 0.05, **, *p* 0.01, ***, *p* 0.001. (**B**) Significantly higher ion abundance of prostaglandin B2, D2 and E2, leukotriene B4 and 12-HETE in HBx experimental cohorts compared to empty control. Mean ± S.D.; p, unpaired student *t*-test, *, *p* 0.05, **, *p* 0.01, ***, *p* 0.001.
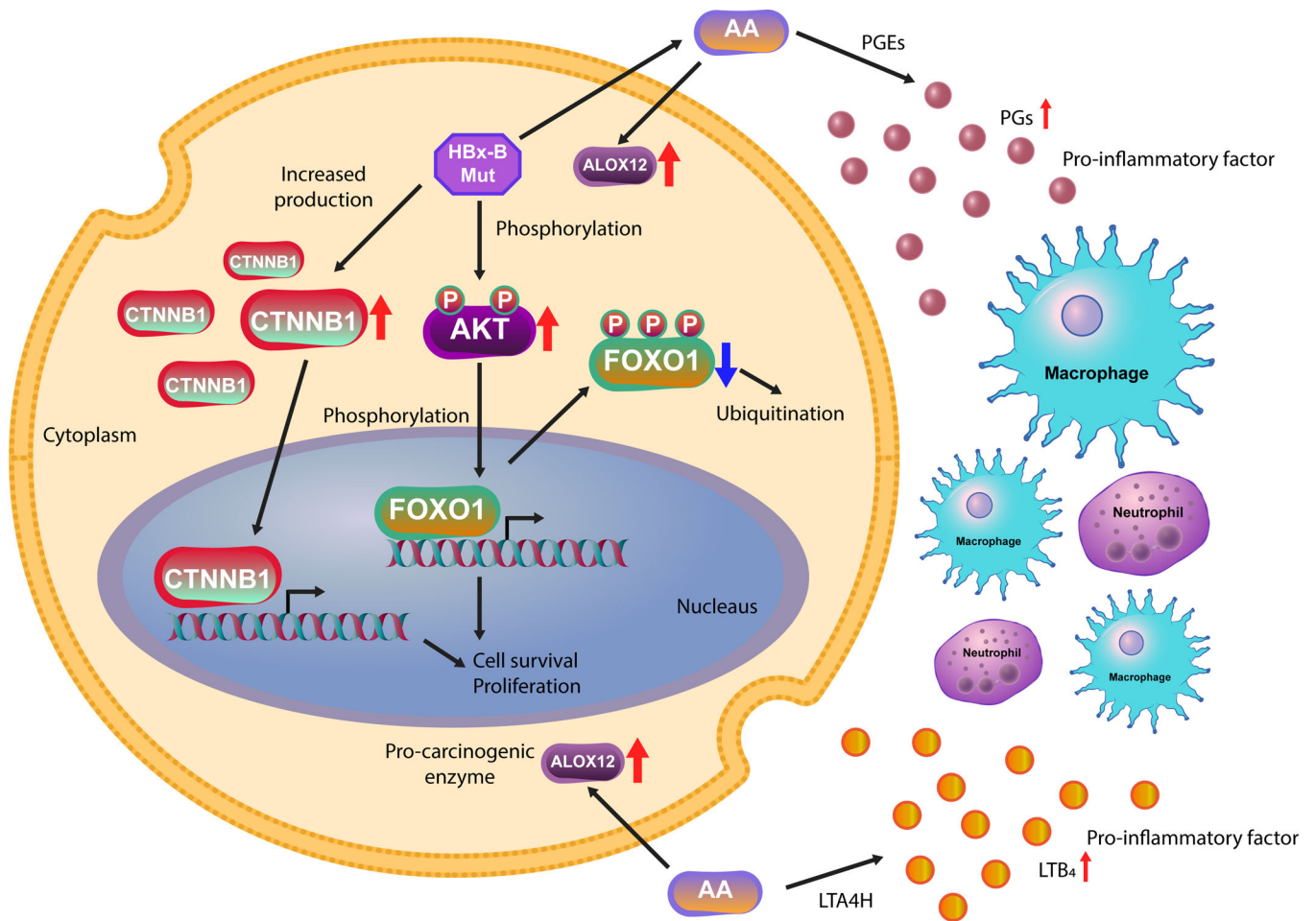
Fig. 5. The schematic image of HBx/AKT/FOXO1 signaling pathway and AA metabolism induced inflammation.

HBx-B Mut promoted tumor progression via phosphorylation of AKT in PI3K/AKT signaling pathway and reduced FOXO1 production. HBx-B Mut gene induced inflammation via AA metabolism by up-regulating *Ptges* and down-regulating gene coded for LTB_4 20-monooxygenase, resulting in accumulation of pro-inflammatory factors, such as prostaglandins (PGs) and LTB_4 around in infected cells (47).